Europium(III) Luminescence and Intramolecular Energy Transfer Studies of Polyoxometalloeuropates

Toshihiro Yamase,* Takeshi Kobayashi, Moriyasu Sugeta, and Haruo Naruke

Research Laboratory of Resources Utilization, Tokyo Institute of Technology, 4259 Nagatsuta, Midori-ku, Yokohama 226, Japan

Received: November 13, 1996; In Final Form: April 12, 1997[⊗]

The photoexcitation in the oxygen-to-metal (M = Nb or W) charge transfer (O→M lmct) bands of two X-ray crystallographically characterized polyoxometalloeuropates, $Na_7H_{19}\{[Eu_3O(OH)_3(H_2O)_3]_2Al_2(Nb_6O_{19})_5\}\cdot 47H_2O$ and $[Eu(H_2O)_8]_3K_2H_3[(GeTi_3W_9O_{37})_2O_3]\cdot 13H_2O$, induced Eu^{3+} emission due to the $^5D_0 \rightarrow {}^7F_J$ ($J = 0-4$) transition with a single-exponential decay. In the latter compound an additional $^5D_1 \rightarrow {}^7F_J$ transition with a weak intensity (with the relative intensity of about 9% of the $^5D_0 \rightarrow {}^7F_J$ emission at 4.2 K) was observed. No observation of the $^5D_1 \rightarrow {}^7F_J$ emission in the former compound was ascribed to the $^5D_1 - {}^5D_0$ cross-relaxation: $Eu^{3+}(^5D_1) + Eu^{3+}(^7F_0) \rightarrow Eu^{3+}(^5D_0) + Eu^{3+}(^7F_3)$. Both nonradiative deactivation of the $^5D_0$ state and intramolecular energy transfer from the O→M lmct states to Eu^{3+} are discussed together with the luminescence properties of four other structurally characterized polyoxotungsto(or molybdo)europates, $Na_9[Eu(W_5O_{18})_2]\cdot 32H_2O$, $K_{15}H_3[Eu_3(H_2O)_3(SbW_9O_{33})(W_5O_{18})_3]\cdot 25.5H_2O$, $[NH_4]_{12}H_2[Eu_4(H_2O)_{16}(MoO_4)(Mo_7O_{24})_4]\cdot 13H_2O$, and $[Eu_2(H_2O)_{12}][Mo_8O_{27}]\cdot 6H_2O$, on the basis of differences in the number of aqua and hydroxo ligands at the first coordination sphere of the Eu^{3+} site, the Eu···Eu distance in the molecule, and the structure of the polyoxometalate ligands among six compounds. A plot of the deviation of the reciprocal $^5D_0$ lifetime from that of $Na_9[Eu(W_5O_{18})_2]\cdot 32H_2O$ containing an anhydrous Eu^{3+} site versus total number of aqua and hydroxo ligands coordinating Eu^{3+} indicates a good linearity irrespective of the coordination geometry, if the mean distance between Eu and aqua or hydroxo oxygen atoms is less than 2.5 Å. The kinetic analysis of the luminescence reveals that the highly symmetrical polyoxometalate ligand favors the effective nonradiative deactivation of the O→M lmct excitation energy due to a small disparity between the O→M lmct excited and ground states and that the energy transfer into the $^5D_0$ and $^5D_1$ states in the polyoxometaloeuropates occurs via the O→M lmct triplet states.

Introduction

The photoexcitation of the oxygen-to-metal charge transfer (O→M lmct) bands of the polyoxometalloeuropates of Mo and W induces Eu^{3+} emission as a result of the intramolecular energy transfer to the $^5D_0$ and $^5D_1$ states of Eu^{3+}.[1−3] The narrow features of the intra-4f electronic transitions are allowed due to mixing with vibrations and/or other electronic states of opposite parity. We have investigated Eu^{3+} emission and crystal structure of luminescent polyoxometalloeuropates such as $Na_9[Eu(W_5O_{18})_2]\cdot 32H_2O$ (**1**),[1g] $K_{15}H_3[Eu_3(H_2O)_3(SbW_9O_{33})(W_5O_{18})_3]\cdot 25.5H_2O$ (**2**),[2a] $[NH_4]_{12}H_2[Eu_4(H_2O)_{16}(MoO_4)(Mo_7O_{24})_4]\cdot 13H_2O$ (**3**),[4] and $[Eu_2(H_2O)_{12}][Mo_8O_{27}]\cdot 6H_2O$ (**4**)[2b] for an insight into the molecular level for the photochemistry and photophysics of rare-earth activated metal oxide phosphors. A variety of inorganic polyoxometalate ligands affect the local symmetry of the coordination geometry of Eu^{3+}, leading to modification of the Eu^{3+} emission properties such as spectrum, lifetime, and energy transfer from the O→M lmct states to Eu^{3+}. The approximate geometries of coordination around Eu^{3+} for **1** and **2** were square antiprism, and for **3** and **4** tricapped trigonal prism. The numbers of aqua ligands coordinating Eu^{3+} for **1**−**4** were 0, 2, 4, and 6, respectively. Figure 1 shows the representation of anions of **1**−**4** as an assembly of linked MO_6 octahedra and the shape of coordination for the Eu atom in the anion. The only luminescence under the O→M lmct band excitation for each complex was the $^5D_0$ (and $^5D_1$)→^7F_J ($J = 0-4$) emission of Eu^{3+} with a single-exponential decay. The decay rate of the $^5D_0 \rightarrow {}^7F_J$ emission increased with increasing number of aqua ligands coordinating the Eu^{3+} atom due to the weak vibronic coupling of the $^5D_0$ state with vibrational states of the high-frequency OH oscillators of the aqua ligand.[5] No observation of the broad O→M (=W, Mo) lmct triplet emission from the polyoxometalate ligands suggests that the energy transfer from the O→M lmct triplet states to Eu^{3+} occurs with a much higher rate ($>10^6$ s^{-1}) than the radiative process of the O→M lmct triplet states.[6] We recently reported the crystal

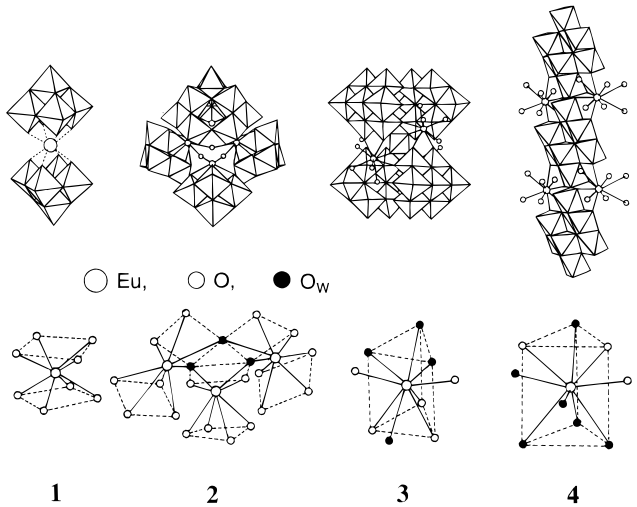

Figure 1. Anion structures of $Na_9[Eu(W_5O_{18})_2]\cdot 32H_2O$ (**1**), $K_{15}H_3[Eu_3(H_2O)_3(SbW_9O_{33})(W_5O_{18})_3]\cdot 25.5H_2O$ (**2**), $[NH_4]_{12}H_2[Eu_4(H_2O)_{16}(MoO_4)(Mo_7O_{24})_4]\cdot 13H_2O$ (**3**), and $[Eu_2(H_2O)_{12}][Mo_8O_{27}]\cdot 6H_2O$ (**4**), and shapes of coordination polyhedra around Eu^{3+}. O_w denotes aqua oxygen atom.

[⊗] Abstract published in *Advance ACS Abstracts,* June 1, 1997.

S1089-5639(96)03786-3 CCC: $14.00

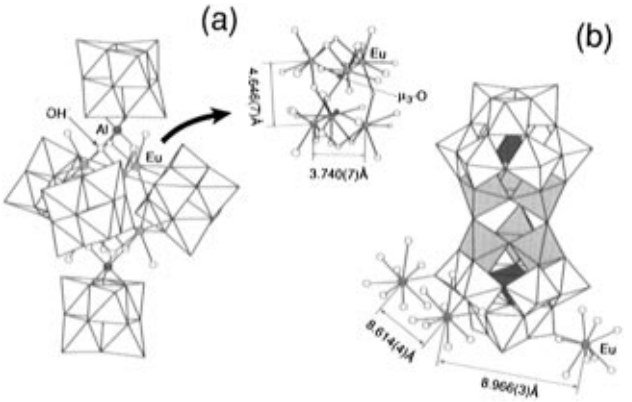

Figure 2. Molecular structures of $\{[Eu_3O(OH)_3(H_2O)_3]_2Al_2(Nb_6O_{19})_5\}^{26-}$ (a) for $Na_7H_{19}\{[Eu_3O(OH)_3(H_2O)_3]_2Al_2(Nb_6O_{19})_5\}\cdot 47H_2O$ (**5**) and $\{[Eu(H_2O)_8]_3[(GeTi_3W_9O_{37})_2O_3]\}^{5-}$ (b) for $K_2H_3\{[Eu(H_2O)_8]_3[(GeTi_3W_9O_{37})_2O_3]\}\cdot 13H_2O$ (**6**). The structures of $[Nb_6O_{19}]^{8-}$ and $[(GeTi_3W_9O_{37})_2O_3]^{14-}$ are given by polyhedral representations which reveal TiO_6 octahedra (shaded) and GeO_4 tetrahedra (black).

structures of $Na_7H_{19}\{[Eu_3O(OH)_3(H_2O)_3]_2Al_2(Nb_6O_{19})_5\}\cdot 47H_2O$ (**5**)[7] and $K_2H_3\{[Eu(H_2O)_8]_3[(GeTi_3W_9O_{37})_2O_3]\}\cdot 13H_2O$ (**6**).[8] The anion of **5** consists of two $[Eu_3O(OH)_3(H_2O)_3]^{4+}$ clusters, two Al^{3+} cations, and five $[Nb_6O_{19}]^{8-}$, and that of **6** is the Keggin-type condensed aggregate, $[GeTi_3W_9O_{37}]^{9-}$. Figure 2 shows schematic representations of the anions of **5** and **6**. The approximate geometry of coordination around Eu^{3+} for **5** was the $EuO_5(OH)_2(H_2O)$ bicapped trigonal prism, which incorporates two OH^- and one aqua ligand in the center, and for **6** the $EuO(H_2O)_8$ tricapped trigonal prism, which incorporates eight aqua ligands. Such structural features strongly differ from **1**−**4** and should have a large difference in luminescence properties. This paper describes the photoluminescence properties of both **5** and **6**, which are discussed together with the luminescence properties of **1**−**4**,[1,2] in terms of both intramolecular energy transfer from the O→M lmct triplet states and nonradiative relaxation of the $^5D_0$ state.

Experimental Section

All of the reagents were of at least analytical grade without further purification. Compounds **1**−**6**[2a,b,4,7−9] and $K_6[Mo_7O_{24}]\cdot 4H_2O$,[10] $K_{5.5}H_{1.5}[SbW_6O_{24}]\cdot 6H_2O$,[11] $K_9H_5[(GeTi_3W_9O_{37})_2O_3]\cdot 16H_2O$,[12] and $K_3Na_4H_2[Tb(W_5O_{18})_2]\cdot 20H_2O$[13] were prepared and purified according to published procedures. Identification was done by comparison of their IR spectra with those previously reported. $[NH_4]_{12}H_2[Tb_4(H_2O)_{16}(MoO_4)(Mo_7O_{24})_4]\cdot 13H_2O$[7] was prepared by replacing $Eu(NO_3)_3\cdot 6H_2O$ as a starting material with $Tb(NO_3)_3\cdot 6H_2O$ in the preparation procedures for **3**.[4]

Diffuse reflectance and IR spectra were recorded on Hitachi 330 and JASCO FT/IR-5000 spectrophotometers at room temperature, respectively. Luminescence and excitation spectra of the sample powder pellet were obtained using a lock-in (NF L1-574) technique. The sample pellet (with a thickness of about 1 mm and a diameter of 10 mm) was prepared by pressing the sample powder under 3×10^7 Pa. The light source for the photoluminescence measurements was a Questek 2320 KrF (248 nm, 100 mJ per pulse) laser, a 500-W xenon lamp (in combination with a Nikon G-25 grating monochromator), or a LDL 20505 LAS dye laser (with LDC 480 dye, 459−510 nm) pumped by a Questek 2320 XeCl (308 nm, 50 mJ per pulse). The luminescence was collected at an angle of 90° to the exciting light and focused onto the entrance slit of a Spex 750M spectrometer (for high-resolution) or a Nikon G-25 grating monochromator that was equipped with Hamamatsu Photonix R636 photomultiplier tube. An absolute wave number accuracy of ±2 cm^{-1} for the high-resolution luminescence spectra was estimated from the dye-laser alignment. Luminescence at low temperatures was measured using a liquid nitrogen Dewar flask (at 77 K) and an Oxford Instruments CF 204 cryostat (at other low temperatures). The time profiles of the luminescence were measured on a LeCloy 9361 digital storage oscilloscope. The quantum yield of the Eu^{3+} (or Tb^{3+}) luminescence for compounds was evaluated by comparing integrated luminescence intensities with that of **1** (exhibiting sharp $^5D_0 \rightarrow {}^7F_J$ ($J = 0-4$) lines with a quantum yield (Φ) = 1.0 at 4.2 K)[1g] under the same arrangement of the pellet. The quantum yield of the O→M lmct triplet emission of $K_9H_5[(GeTi_3W_9O_{37})_2O_3]\cdot 16H_2O$ was estimated by comparing integrated luminescence intensities with that of $K_{5.5}H_{1.5}[SbW_6O_{24}]\cdot 6H_2O$ (exhibiting a broad emission spectrum peaking at 520 nm with $\Phi = 0.61$ at 4.2 K).[6] No observable part of the original intensity of the incident light was transmitted through the sample pellet.

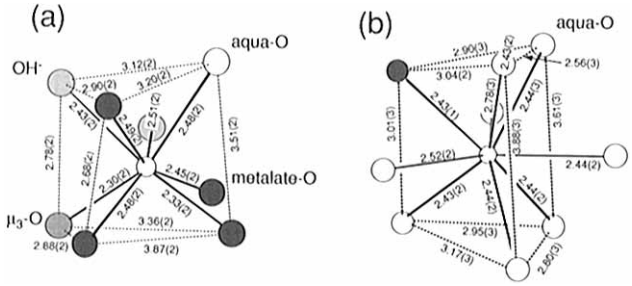

Figure 3. The 8-fold bicapped trigonal-prismatic (a) and 9-fold tricapped-prismatic (b) geometries of the coordination polyhedra around Eu^{3+} in **5** and **6**, respectively.

Results

Structure of Eu^{3+} Sites. Schematic representations of the approximate geometry of coordination around Eu^{3+} for **5** ($P\bar{1}$, $Z = 2$, $a = 23.15(2)$ Å, $b = 28.31(2)$ Å, $c = 19.32(2)$ Å, $\alpha = 107.03(6)°$, $\beta = 113.44(10)°$, $\gamma = 100.81(8)°$)[7] and **6** ($P2_1/m$, $Z = 2$, $a = 13.177(2)$ Å, $b = 18.645(3)$ Å, $c = 21.800(3)$ Å, $\beta = 99.82(1)°$)[8] are shown in Figure 2, where the atomic distances and angles are averaged for six Eu^{3+} sites in **5** and for three Eu^{3+} sites in **6**. The average distances between Eu and oxygen atoms for $[Nb_6O_{19}]^{8-}$, μ_3-O, OH^-, and aqua ligands at each $EuO_5(OH)_2(H_2O)$ site of **5** are 2.44(1), 2.30(1), 2.47(1), and 2.48(1) Å, respectively. The μ_3-O atom is shared by three Eu^{3+} and the hydroxo oxygen atom is shared by two Eu^{3+} and one Al^{3+} (Figure 2).[7] The coordination geometry is best described as bicapped trigonal prismatic, one trigonal face being defined by one oxygen from each of $[Nb_6O_{19}]^{8-}$, OH^-, and aqua oxygen (O_w) ligands and other trigonal face by one oxygen from each of two $[Nb_6O_{19}]^{8-}$ and μ_3-O ligands. The two approximately rectangular faces are then capped by the other oxygen of each $[Nb_6O_{19}]^{8-}$ and another OH^-. At each $EuO(H_2O)_8$ site of **6**, the average distances between Eu and oxygen atoms for the $[(GeTi_3W_9O_{37})_2O_3]^{14-}$ and aqua ligands are 2.43(1) and 2.49(1) Å, respectively. The (terminal) oxygen atom from $[(GeTi_3W_9O_{37})_2O_3]^{14-}$ defines one of the three oxygen atoms in one trigonal face for the $EuO(H_2O)_8$ coordination geometry described as tricapped trigonal prismatic. Although both $EuO_5(OH)_2(H_2O)$ and $EuO(H_2O)_8$ sites (Figure 3) give approximate local symmetry of C_{2v}, these are distorted to C_1 symmetry due to crystal packing forces. The Eu···Eu distances in the $[Eu_3O(OH)_3(H_2O)_3]^{4+}$ half-core for **5** are 3.740(7)−3.777(5) Å [average, 3.756(2) Å],[7] which are about 1.3 Å shorter than those in the singly bridged trimeric $[Eu_3(H_2O)_3]^{9+}$ core for **2**, where the Eu···Eu distances were 5.015(5)−5.067(4) Å [average, 5.050(3) Å].[2a] Two half-cores are linked via one bridging oxygen atom from each of three equatorial $[Nb_6O_{19}]^{8-}$ anions

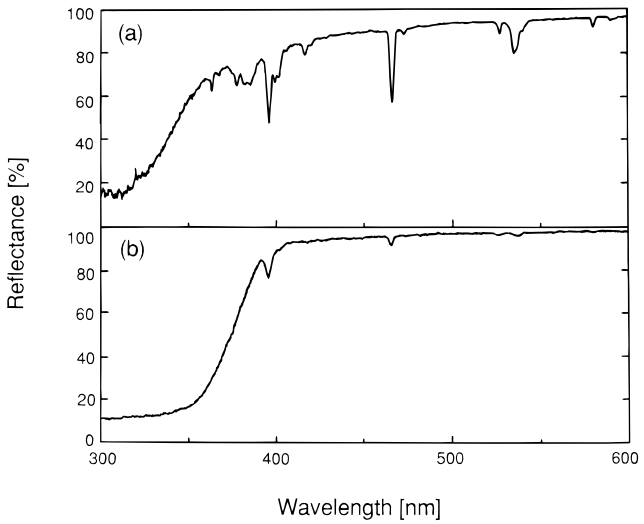

Figure 4. Diffuse reflectance spectra of **5** (a) and **6** (b) at 300 K.

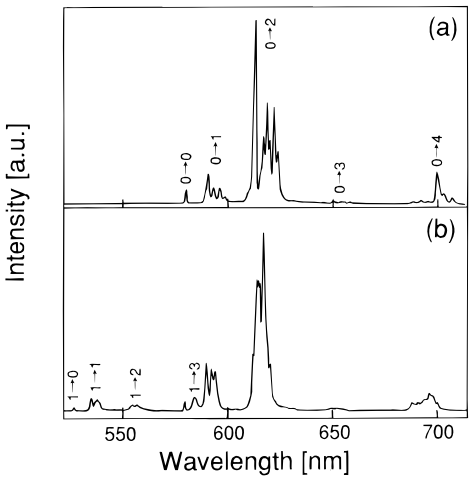

Figure 5. Low-resolution emission spectra of **5** (a) and **6** (b) solids. Excitation wavelength is 248 nm at 4.2 K. Numbers indicate $J \rightarrow J'$ for the $^5D_J \rightarrow {}^7F_J$, transitions.

(Figure 2), with Eu···Eu distances of 4.609(6)−4.763(6) Å [average, 4.75(2) Å for the two Eu atoms sharing a common O atom and 4.64(2) Å elsewhere].[7] The nearest Eu···Eu distances for **6** are long; the shortest Eu···Eu distance [7.631(3) Å] is observed for neighboring molecules, and the Eu···Eu distances in the same molecule are 8.614(4) and 8.966(3) Å (Figure 2).[8]

Diffuse Reflectance and Luminescence Spectra. The diffuse reflectance spectra of **5** and **6**, recorded at room temperature, show the intense broad bands of the O→M lmct absorption and the sharp lines corresponding to the transitions within the $4f^6$ shell of Eu^{3+}, as shown in Figure 4. The optical absorption edges for the $[Nb_6O_{19}]^{8-}$ and $[(GeTi_3W_9O_{37})_2O_3]^{14-}$ ligands lie at 350 ± 10 and 380 ± 10 nm, respectively. The diffuse reflectance spectrum of **5** visualizes more lines of the f−f transitions than that of **6**. In **5** the $^7F_0 \rightarrow {}^5D_{0,1,2,3}$ transitions occur at about 581, 527, 466, and 416 nm, respectively. Each line accompanies the transition due to the population of the $^7F_1$ state with a separation of about 300 cm^{-1}; $^7F_1 \rightarrow {}^5D_{0,1,2,3}$ transitions are at about 590, 536, 473, and 420 nm, respectively. The sharp lines at about 396, 384, 377, 363, and 320 nm may be assigned to the $^7F_0 \rightarrow {}^5L_{6,7,8,9}$ and ^5H multiplet transitions, respectively.[14] In **6** the $^7F_0 \rightarrow {}^5D_{1,2}$, $^7F_1 \rightarrow {}^5D_{1,2}$, and $^7F_0 \rightarrow {}^5L_6$ lines appear at about 526, 466, 538, 472, and 395 nm, respectively.

Figure 5 shows the low-resolution emission spectra of **5** and **6** at 4.2 K under excitation by the 248-nm light corresponding to the O→Nb (or W) lmct bands. The $^5D_0 \rightarrow {}^7F_{0,1,2,3,4}$ lines are clearly visible at the range 580−710 nm. In **6** the $^5D_1 \rightarrow {}^7F_{0,1,2,3}$ transitions at the range 526−585 nm are observed on the 4.2 K spectrum, where the weak $^5D_1 \rightarrow {}^7F_4$ transitions are superimposed in the region of the strong $^5D_0 \rightarrow {}^7F_2$ transitions. Table 1 shows the relative intensities of $^5D_0 \rightarrow {}^7F_J$ emission at 4.2 K for **5** and **6**, together with those for **1**−**4** for comparison.[1g,2a−c] The $^5D_0 \rightarrow {}^7F_J$ luminescence of the anhydrous Eu^{3+} site in **1** exhibited the highest intensity (with doublet lines) of the $^5D_0 \rightarrow {}^7F_1$ emission.[1] Such a $^5D_0$ emission pattern is different from that of the hydrous Eu^{3+} site in **2**−**6**, where the $^5D_0 \rightarrow {}^7F_2$ emission corresponding to the electric-dipole transition exhibits the highest intensity with multiplet lines for a single Eu^{3+} center. This suggests that the presence of the aqua ligand in the first coordination sphere causes a dramatic increase in the magnitude of the hypersensitive $^5D_0 \rightarrow {}^7F_2$ manifold. An increase in temperature resulted in no significant change in the relative intensity of the $^5D_0 \rightarrow {}^7F_J$ emission. The $^5D_1 \rightarrow {}^7F_{0,1,2,3}$ emission for **6**, in which the relative intensity of the $^5D_1 \rightarrow {}^7F_1$ transition is the highest, is very weak in intensity, and its total yield is about 9% of the $^5D_0 \rightarrow {}^7F_J$ emission at 4.2 K. The high-resolution emission spectra at 4.2 K within the various $^5D_J \rightarrow {}^7F_J$ band systems for **5** and **6** are shown in Figure 6. In **5**, where six crystallographically different Eu^{3+} sites exist (Figure 2), the existence of a broad asymmetric peak of the $^5D_0 \rightarrow {}^7F_0$ transition is taken as evidence that at least three Eu^{3+} sites are responsible for the series of luminescence transitions, since the $^5D_0 \rightarrow {}^7F_0$ transition at about 580 nm cannot be split by any crystal field. This leads to the observation of a large amount of lines and inhomogeneous broadening. However, the different lines in the $^5D_0 \rightarrow {}^7F_{1,2,3,4}$ regions could not be assigned individually to these three different sites. In **6** an observable single $^5D_0 \rightarrow {}^7F_0$ peak at 579.6 nm suggests that two crystallographically different Eu^{3+} sites are almost equivalent spectroscopically. This is supported by the observation of three $^5D_0 \rightarrow {}^7F_1$ peaks, seven $^5D_0 \rightarrow {}^7F_3$ peaks, and nine $^5D_0 \rightarrow {}^7F_4$ peaks, which is in good agreement with the crystallographic site symmetry of C_s or C_1 for the Eu^{3+} site in **6** (Figure 3b).[8] $^5D_0 \rightarrow {}^7F_2$ lines were not identified due to complexity from the superimposed $^5D_1 \rightarrow {}^7F_4$ lines in this region. There seemed to be no peak assigned as vibronic in nature, since all of the peaks exhibited similar temperature dependence.

TABLE 1: Relative Intensities of the $^5D_0 \rightarrow {}^7F_J$ Emissions of Eu^{3+} at 4.2 K for 1−6

terminal level	**1**[1g]	**2**[2a]	**3**[2c]	**4**[2b]	**5**	**6**
$^7F_0$	∼0	2	1	∼0	1.3	0.3
$^7F_1$	50	18	13	15	9.9	17.2
$^7F_2$	18	69	74	72	78.2	71.4
$^7F_3$	5	3	1	2	1.0	1.0
$^7F_4$	27	8	11	11	9.6	10.1

[a] Relative intensities of the $^5D_0 \rightarrow {}^7F_J$ emissions for **3** were those at 77 K, because of its degradation at 4.2 K.[2c]

The low-resolution excitation spectra of the $^5D_0 \rightarrow {}^7F_2$ emission for **5** and **6** are shown in Figures 7 and 8, respectively, where the spectra at 4.2, 77, and 300 K are represented. Each excitation spectrum consists of broad O→M lmct bands at $\lambda <$ 350 nm and sharp f−f lines. The excitation curves in the region $\lambda <$ 350 nm were corrected to signals for a constant photon flux at about 395 nm, where a strong, sharp $^7F_0 \rightarrow {}^5L_6$ transition line appeared. The most remarkable difference in the excitation spectra between **5** and **6** is a slight shift to shorter wavelengths of the O→M lmct bands with accompanying additional $4f^6$ lines (most likely the $^7F_0 \rightarrow {}^5L_{7,8,9}$ and ^5H multiplet transitions) in **5**; thresholds of the O→Nb and W (or Ti) lmct bands are around 330 and 350 nm, respectively. Excitation at different wavelengths of the O→M lmct and $^7F_0 \rightarrow {}^5D_{1,2,3}$ bands made no difference in the emission spectrum. The high-temperature

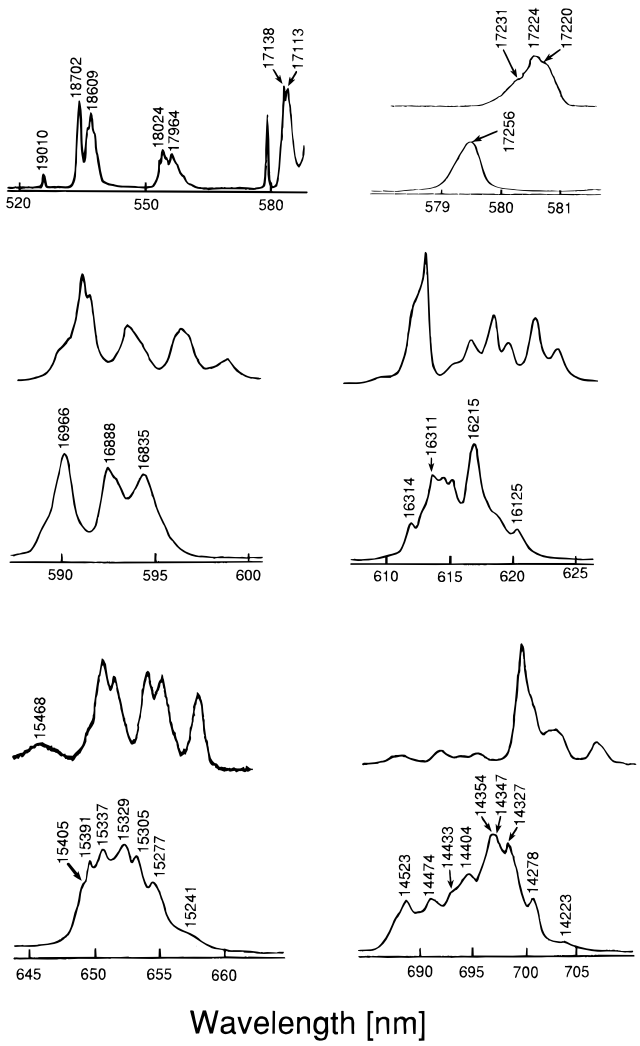

Figure 6. High-resolution emission spectra of **5** (upper set) and **6** (lower set) solids at 4.2 K. The positions of the emission lines are indicated in frequency units.

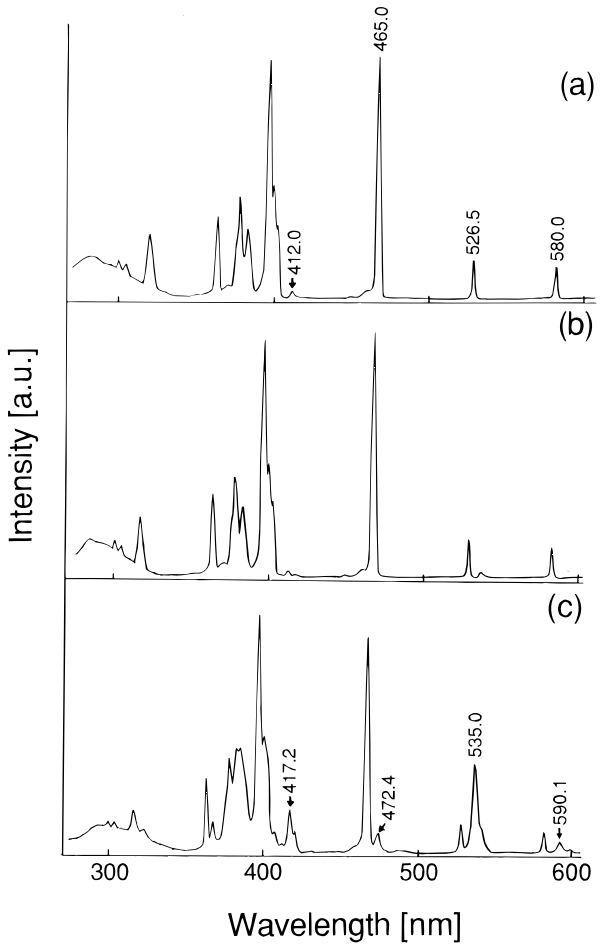

Figure 7. Excitation spectra of **5** at 4.2 (a), 77 (b), and 300 K (c) under low resolution for the $^5D_0 \rightarrow {}^7F_2$ transitions (at 613 nm). Some of the positions of the lines are indicated in nanometer units.

excitation spectra of the $^5D_0 \rightarrow {}^7F_2$ emission exhibits the $^7F_1 \rightarrow {}^5D_{0,1,2,3}$ lines at 590.1, 535.0, 472.4, and 417.2 nm with an energy separation of about 300 cm^{-1} from the $^7F_0 \rightarrow {}^5D_{0,1,2,3}$ lines at 580.0, 526.5, 465.0, and 412.0 nm. This feature corresponds to the reflection spectra at room temperature (Figure 4). The observable $^5D_0 \rightarrow {}^7F_3$ line at 646 nm in **5** (Figure 6) makes the energy difference ($\sim$1755 cm^{-1}) from the $^5D_0 \rightarrow {}^7F_0$ line, which is very close to the energy difference ($\sim$1750 cm^{-1}) between the $^5D_1$ and $^5D_0$ states (Figure 7). On the other hand, in **6** there was no $^5D_0 \rightarrow {}^7F_3$ line at the range 645−646 nm. Thus, no observation of the $^5D_1 \rightarrow {}^7F_J$ emission for **5** (Figures 5 and 6) can be attributed to the quenching of higher level emission by cross-relaxation between the $^5D_1$ and $^7F_0$ states: the $^5D_1$ emission is quenched by transferring the energy difference $^5D_1 - {}^5D_0$ which is promoted from $^7F_0$ to the $^7F_3$ level (eq 1). In the cross-relaxation the higher energy emission is quenched in favor of the lower energy level emission.[15,16]

$$Eu^{3+}(^5D_1) + Eu^{3+}(^7F_0) \rightarrow Eu^{3+}(^5D_0) + Eu^{3+}(^7F_3) \quad (1)$$

Temperature Dependences of Emission Decay and Intensity. The decay pattern of the $^5D_0 \rightarrow {}^7F_J$ luminescence for **5** and **6** was a single exponential, and their luminescence lifetimes (τ) are approximately 0.31−0.32 and 0.14−0.15 ms, respectively, which almost are both temperature- and excitation wavelength-independent. The short luminescence decay of **6** compared with **5** can be predicted from the high number of

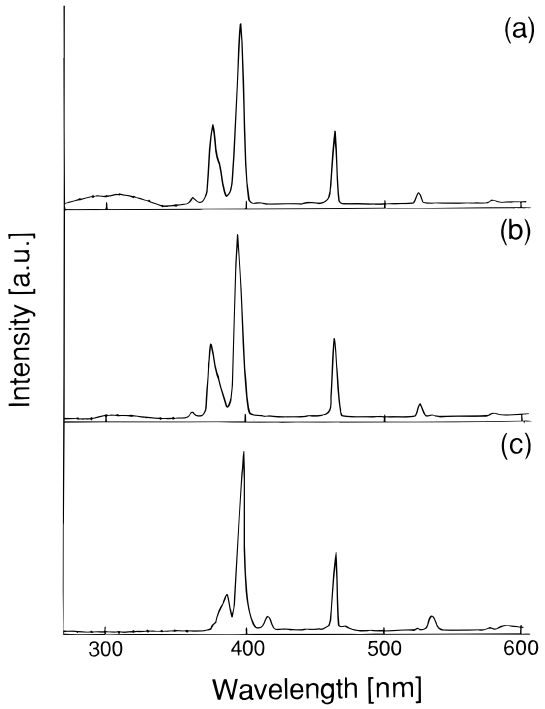

Figure 8. Excitation spectra of **6** at 4.2 (a), 77 (b), and 300 K (c) under low resolution for the $^5D_0 \rightarrow {}^7F_2$ transitions (at 617 nm).

aqua ligands in the Eu^{3+} coordination sphere.[2e,5] The decay of the $^5D_1 \rightarrow {}^7F_J$ luminescence of **6** is strongly temperature-dependent [for example, τ(4.2 K) = 14 ± 2 μs and τ(77 K) = 8 ± 1 μs], most probably because of the temperature dependence

TABLE 2: Approximate Coordination Geometry (CG) around Eu^{3+}, Average (TC) of the Total Charge of Ligands Bound to Eu^{3+}, Number (n) of Aqua (or Hydroxo) Ligands Bound to Eu^{3+}, and τ (in ms) and Φ of the $^5D_0 \rightarrow {}^7F_J$ Emission upon O→M lmct Band Excitation for 1−6

	1[1g]	**2**[2a]	**3**[2c]	**4**[2b]	**5**	**6**
CG	s.a.	s.a.	t.t.	t.t.	b.t.	t.t.
TC	12	9	6.5	3	7.3	4.7
n	0	2	4	6	1, (2)[b]	8
τ						
4.2 K	3.7	1.1 ± 0.2	*c*	0.16	0.32 ± 0.01	0.15 ± 0.01
77 K	3.3	1.1 ± 0.2	0.24 ± 0.02	0.17 ± 0.01	0.31 ± 0.01	0.14 ± 0.01
300 K	2.8	1.1 ± 0.2	0.20 ± 0.01	0.17 ± 0.01	0.31 ± 0.02	0.14 ± 0.01
Φ						
4.2 K	0.99	0.55	*c*	0.034	0.085 ± 0.001	$(7 \pm 1) \times 10^{-4}$
77 K	0.90	0.51	0.12	0.029	0.042 ± 0.001	$(2 \pm 1) \times 10^{-4}$
300 K	0.80	0.25	0.07	0.013	0.009 ± 0.001	

[a] s.a. = square anti-prismatic, t.t. = tricapped trigonal-prismatic, b.t. = bicapped trigonal prismatic. [b] Number of hydroxo ligands. [c] Measurements at 4.2 K for **3** were not done due to its degradation.

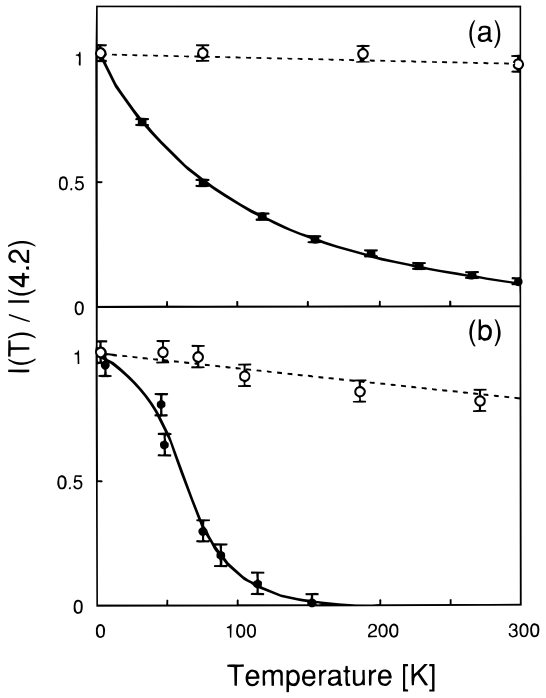

Figure 9. Total intensity of the emission normalized by $I(4.2)$ as a function of temperature for **5** (a) and **6** (b). The solid curve is for the O→M lmct band (248 nm) excitation, and the dashed curve is for the $^7F_0 \rightarrow {}^5L_6$ line (395 nm) excitation.

of the nonradiative conversion from $^5D_1$ to $^5D_0$.[16] Temperature dependence of the Eu^{3+} emission intensity differs in the excitation wavelength: the decreasing effect of the O→M lmct band excitation on the emission intensity with increasing temperature was larger than the f−f band excitation. This can also be demonstrated by the temperature dependence of the excitation spectra (Figures 7 and 8). Figure 9 shows the normalized total intensity $I(T)/I(4.2)$ obtained by both O→M lmct and f−f band excitations as a function of temperature for **5** and **6**. The quantum yield (Φ) of the $^5D_0 \rightarrow {}^7F_J$ emission at 4.2 K under 248-nm light excitation for **5** is 0.085 ± 0.001 and that for **6** is $(7 \pm 1) \times 10^{-4}$. A small temperature dependence of the luminescence intensity under the f−f band excitation is predicted by the small effect of τ on the temperature, excluding the possibility of the thermal expansion of the $^5D_0$ state to result in a high rate of nonradiative deactivation. On the other hand, the large temperature dependence of the luminescence intensity under O→M lmct band excitation for **5** and **6** is associated with the thermal relaxation of the O→M lmct states to compete with the energy transfer to Eu^{3+} in the lattice. The temperature dependence of the normalized total intensity under O→M lmct band excitation for **6** is stronger than for **5**: the normalized total intensity at 4.2 K for **5** is about 10 times larger than at 300 K, while the normalized total intensity at 4.2 K for **6** is about 50 times larger than at 150 K; there is no emission above 200 K.

Discussion

Coordination of Aqua and Hydroxo Ligands. The number (n) of aqua ligand in the first coordination sphere at the central Eu^{3+} site is relevant to the lifetime (τ) of the $^5D_0$ state. τ and Φ of the $^5D_0$ luminescence on O→M lmct band photoexcitation for **1**−**6** at three temperatures 4.2, 77, and 300 K are listed in Table 2, where n, the approximate geometry (GC) of the coordination polyhedron around Eu^{3+}, and the average (TC) of the total charge of the ligands bound to Eu^{3+} for **1**−**6** are also given. As shown in Table 2, the Eu^{3+} site for high TC values (≥ 9) favors the square antiprismatic geometry with $n \leq 2$, and for low TC values (≤ 6.5) the tricapped trigonal prismatic geometry with $n \geq 4$. This is associated with the contraction of the coordination sphere due to a nephelauxetic effect.

A method to estimate n in Eu^{3+} complexes with an uncertainty of 0.5 has been given by

$$n = 1.05(\tau_{H_2O}{}^{-1} - \tau_{D_2O}{}^{-1}) \qquad (2)$$

where $\tau_{H_2O}{}^{-1}$ and $\tau_{D_2O}{}^{-1}$ are the reciprocal experimental lifetimes in H_2O and D_2O surroundings in $(ms)^{-1}$, respectively.[5] This is based on the linear plots of the reciprocal lifetimes of the $^5D_0$ state versus n for a variety of structurally well-characterized aminopolycarboxylatoeuropate complexes. Since τ_{D_2O} corresponds to the $^5D_0$ lifetime of the complex with $n = 0$, it is reasonable to provide $\tau_{D_2O} = 3.3$ ms, the $^5D_0$ lifetime at 77 K for **1**.[1g] Thus, the method was applied to **1**−**6** (at 77 K) solids showing square anti-, bicapped trigonal-, and tricapped trigonal-prismatic coordination geometries of Eu^{3+}. Figure 10 shows a plot of the difference in reciprocal $^5D_0$ lifetimes at 77 K between **2**−**6** and **1**, $\Delta\tau_{obs}{}^{-1}$, versus the crystallographically determined number of aqua ligands in the first coordination spheres, n. The solid line in Figure 10 indicates the relationship (given by eq 2) obtained for various aminopolycarboxylatoeuropate complexes.[5] As shown in Figure 10, $\Delta\tau_{obs}{}^{-1}$ values for **2**, **5**, and **6** correspond to n values of 0.5, 3, and 7 in eq 2, respectively. The deviation from eq 2 for **2** and **6** suggests that the Eu^{3+}−H_2O coupling per H_2O molecule is considerably weak to have the Eu−O_w distance lengthened. Table 3 summarizes Eu−O, Eu−O_w bond distances, the shortest Eu···Eu distances, and Eu−O−M bond angles for **1**−**6**.[1,2,4,7,8] In **2** the Eu−O_w distances of 2.51(3)−2.64(3) Å [average 2.56(2) Å] are longer than the average Eu−O_w distances [2.49(1) and 2.48(1) Å] observed for **3** and **4**, where eq 2 is followed. Similarly, in **6** one (capping)

TABLE 3: Eu−O (O_w or O_H) and the Shortest Eu···Eu Distances (in Å) and Eu−O−M Bond Angles (in deg) for 1−6[a]

	1[1g]	**2**[2a]	**3**[4]	**4**[2b]	**5**[7]	**6**[8]
Eu−O	2.39(3)−2.46(3)	2.29(3)−2.51(3)	2.38(1)−2.48(2)	2.41(1)−2.58(1)	2.28(4)−2.51(3)	2.42(3)−2.43(3)
mean	2.43(1)	2.41(1)	2.43(1)	2.46(1)	2.39(1)	2.43(1)
Eu−O_w			2.43(2)−2.59(2)	2.43(2)−2.61(1)	2.41(3)−2.54(3)	2.40(3)−2.59(3)
mean			2.49(1)	2.48(1)	2.48(2)	2.44(1)
		2.51(3)−2.64(3)				2.59(3)−2.88(5)
mean		2.56(2)				2.78(3)
Eu−O_H					2.41(3)−2.54(3)	
mean					2.47(1)	
Eu···Eu	11.484(5)	5.015(5)	6.158(2)	6.251(3)	3.740(7)	7.631(3)
Eu−O−M	128(1)−132(1)	122(2)−127(2)			98(1)−106(1)[b]	
		149(2)−153(2)	147(1)−157(8)	147(1)−158(1)	140(2)−143(2)[b]	
						160(2)−171(1)

[a] O_w = aqua oxygen, O_H = hydroxo oxygen. [b] In **5** the Eu−O−Nb bond angles of about 100° are for μ_3- and μ_4-atoms originated from the bridging oxygens in the $[Nb_6O_{19}]^{8-}$ ligand, and those of about 142° are for μ_2-atoms originated from the terminal oxygens.

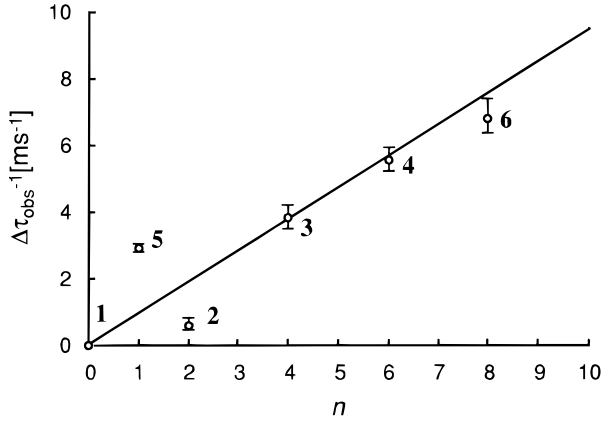

Figure 10. Plots of the difference in the observed reciprocal emission lifetimes at 77 K, $\Delta\tau_{obs}^{-1}$, between **2**−**6** and **1** (open circles) versus the crystallographically determined numbers of water molecules in the first coordination spheres of Eu^{3+}, *n*. The solid line indicates the relationship of $n = 1.05\Delta\tau_{obs}^{-1}$ given by eq 2.

of eight O_w atoms gives a long distance from the central Eu^{3+} atom of 2.59(3)−2.88(5) Å [average 2.78(3) Å], compared with other O_w atoms in the Eu−O_w distances of 2.40(3)−2.59(3) Å [average 2.44(1) Å] (Figure 3). On the other hand, the deviation from eq 2 for **5**, where two hydroxo ligands coordinate Eu^{3+} with Eu−O distances of 2.41(3)−2.54(3) Å [average 2.47(1) Å], clearly indicates a strong contribution of the vibrational states of the high-frequency OH oscillators of two hydroxo ligands to the $^5D_0$ lifetime as well as an aqua ligand. Although eq 2 should be used with care, especially for the case of the long Eu−O_w distances of more than 2.6 Å, the $\Delta\tau_{obs}^{-1}$ value for the polyoxometalloeuropates is sufficiently useful to enable the prediction of the number of aqua and hydroxo ligands coordinating Eu^{3+}, irrespective of the coordination geometry, for compounds not amenable to study by single-crystal X-ray methods.

Kinetics of Energy Transfer. If the exchange interaction between the Eu^{3+} sites in the lattice with shortest Eu···Eu distances of <5 Å becomes effective, the energy transfer rate between the Eu^{3+} sites would be on the order of 10^7 s^{-1}, which is much larger than the radiative rate of 10^2−10^3 s^{-1} (as shown below).[17] However, the observation of a simple exponential decay of the $^5D_0$ emission of **2**, **3**, and **5** (with Eu···Eu distances of <6.15 Å) with moderate quantum yield (Tables 2 and 3)[2] implies that there is no energy migration between the two Eu^{3+} sites at all. The magnetic-dipole character of the $^5D_0 \rightarrow {}^7F_1$ transition lets us consider the radiative rate of this transition to be almost independent of the geometry of the Eu^{3+} surroundings, as long as the mixing of the electric-dipole character into the $^5D_0 \rightarrow {}^7F_1$ transition is small.[18] Therefore, it may be meaningful to use the $^5D_0 \rightarrow {}^7F_1$ magnetic-dipole transition as a standard in order to estimate the radiative rate for **1**−**6**.[19] We take **1** as a reference, since **1** comprising the anhydrous Eu^{3+} site exhibited a high quantum yield (∼1.0) of the emission with a large distribution of the $^5D_0 \rightarrow {}^7F_1$ transition in the luminescence spectrum on O→W lmct band excitation (Tables 1 and 2), and its optical absorption edge is not too much different from other complexes.[1d,e,g] The radiative rate (k_{rad}) for **1** is 2.7×10^2 s^{-1} (=1/3.7 ms) at 4.2 K, and the $^5D_0 \rightarrow {}^7F_1$ transition contains 0.50 of the total emission (Table 1). Thus, the $^5D_0 \rightarrow {}^7F_1$ rate is 1.35×10^2 s^{-1}. In other complexes the amount of the $^5D_0 \rightarrow {}^7F_1$ emission is less intensive. Therefore, k_{rad} for **5** is 1.4×10^3 ($=1.35 \times 10^2/0.099$) s^{-1} (Table 1). Since the experimental decay rate of the emission for **5** is $(3.1 \pm 0.1) \times 10^3$ s^{-1} [=1/(0.32 ± 0.01) ms), we estimate a nonradiative rate (k_{nr}) of $(1.7 \pm 0.1) \times 10^3$ [$=(3.1 \pm 0.1) \times 10^3 - 1.4 \times 10^3$] s^{-1} and then the ratio (η_{rad}) of the radiation for the $^5D_0$ state to be 0.45 ± 0.01 [$=1.4 \times 10^3/(3.1 \pm 0.1) \times 10^3$]. With these data the quantum yield (Φ_{et}) of the overall energy transfer from the O→M lmct states to the $^5D_0$ state (through the $^5D_1$ state in part) is calculated as 0.18 ± 0.01 [$=(0.085 \pm 0.001)/(0.45 \pm 0.01)$] (Table 2). Table 4 surveys the evaluated values of k_{rad}, k_{nr}, η_{rad}, and Φ_{et} at 4.2, 77, and 300 K for **1**−**6**.

The decrease in Φ_{et} with an increase in temperature has been elucidated by the d^1 hopping delocalization in the polyoxometalate ligand, which depends on the configuration of both M−O−M and Eu−O−M linkages.[2] The thermal deactivation of the O→M lmct states due to the d^1 hopping is based on the small disparity of electronic configurations between the excited and ground states, which is reflected by the bond angle of the M−O−M or Eu−O−M linkage. The photoexcitation into the O→M lmct bands would allow the hopping of the d^1 electron to the Eu^{3+} site via the Eu−O−M linkage involving the 2p orbital of the bridging oxygen atom, if the Eu−O−M bond angles are about 150°, since the fπ−pπ−dπ orbital mixing on the Eu−O−M linkage would be possible with a mode similar to the dπ−pπ−dπ orbital mixing for the corner-sharing MO_6 octahedra with M−O−M bond angles of about 150°.[2] The polyoxometalate ligands consisting of only edge-sharing MO_6 octahedra with M−O−M bond angles of about 100° give a small temperature dependence of Φ_{et} (with its high value) due to the localization of the d^1 electron at the MO_6 octahedron, as exemplified by **1**. The Eu−O−M bond angle of about 150° elucidates a strong temperature dependence of Φ_{et} for **2**, **3**, and **4** (Tables 3 and 4), as discussed previously.[2b,e] A low value of Φ_{et} [$=(0.24 \pm 0.01)$ at 4.2 K] for **4** compared with **3** [$\Phi_{et} = (0.48 \pm 0.04)$ at 77 K] is ascribed to the additional factor of the small disparity between the excited and ground O→M lmct states, which arises from the nearly linear Mo−O−Mo linkage [179.9(1)° with the Mo−O distance at 1.88(1) Å] involved in joining γ-$[Mo_8O_{26}]^{4-}$ anions through the 2-fold O atom.[2b] It should be recalled that the quantum yield of the O→M lmct

TABLE 4: Radiative Rate (k_{rad} in s^{-1}), Nonradiative Rate (k_{nr} in s^{-1}), and Ratio (η_{rad}) of Radiation of the $^5D_0$ State of Eu^{3+} and Quantum Yield (Φ_{et}) of the Overall Energy Transfer from O→M lmct States to the $^5D_0$ State (through the $^5D_1$ State in Part) for 1−6[a]

	1	2	3	4	5	6
k_{rad}	2.7×10^2	7.5×10^2	1.1×10^3	9.0×10^2	1.4×10^3	7.9×10^2
k_{nr}						
4.2 K	∼0	$(1.9 \pm 1.7) \times 10^2$		5.4×10^3	$(1.7 \pm 0.1) \times 10^3$	$(5.9 \pm 0.4) \times 10^3$
77 K	3×10	$(1.9 \pm 1.7) \times 10^2$	$(3.2 \pm 0.3) \times 10^3$	$(5.0 \pm 0.3) \times 10^3$	$(1.8 \pm 0.1) \times 10^3$	$(6.4 \pm 0.5) \times 10^3$
300 K	9×10	$(1.9 \pm 1.7) \times 10^2$	$(4.0 \pm 0.2) \times 10^3$	$(5.0 \pm 0.3) \times 10^3$	$(1.8 \pm 0.2) \times 10^3$	$(6.4 \pm 0.5) \times 10^3$
η_{rad}						
4.2 K	1.0	0.83 ± 0.15		0.14 ± 0.01	0.45 ± 0.01	0.12 ± 0.01
77 K	0.90	0.83 ± 0.15	0.25 ± 0.02	0.15 ± 0.01	0.43 ± 0.01	0.11 ± 0.01
300 K	0.75	0.83 ± 0.15	0.21 ± 0.01	0.15 ± 0.01	0.44 ± 0.03	0.11 ± 0.01
Φ_{et}						
4.2 K	1.0	0.69 ± 0.12		0.24 ± 0.01	0.19 ± 0.01	$(6 \pm 1) \times 10^{-3}$
77 K	1.0	0.64 ± 0.12	0.48 ± 0.04	0.19 ± 0.01	0.09 ± 0.01	$(2 \pm 1) \times 10^{-3}$
300 K	0.94	0.31 ± 0.06	0.33 ± 0.02	0.08 ± 0.01	0.02	

[a] Since the relative intensities of $^5D_0 \rightarrow {}^7F_J$ emission were hardly changed with a variety of temperature, k_{rad} was evaluated to be independent of the temperature.

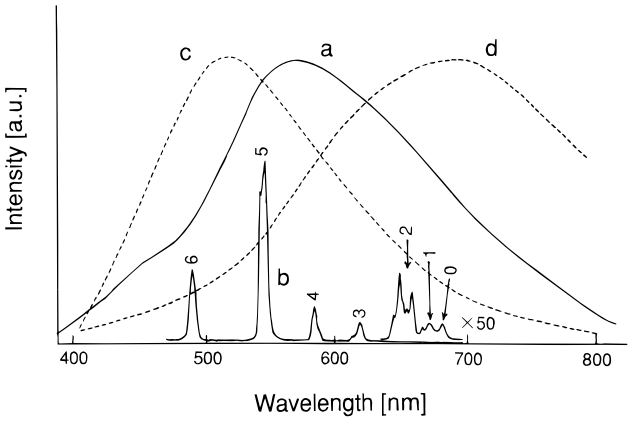

Figure 11. Photoluminescence spectra of $K_9H_5[(GeTi_3W_9O_{37})_2O_3]\cdot 16H_2O$(a), $[NH_4]_{12}H_2[Tb_4(H_2O)_{16}(MoO_4)(Mo_7O_{24})_4]\cdot 13H_2O$ (b), $K_{5.5}H_{1.5}[SbW_6O_{24}]\cdot 6H_2O$ (c), and $K_6[Mo_7O_{24}]\cdot 4H_2O$ (d) under O→M lmct band (248 nm) excitation. The $[NH_4]_{12}H_2[Tb_4(H_2O)_{16}(MoO_4)(Mo_7O_{24})_4]\cdot 13H_2O$ solid, which was degraded at 4.2 K, was measured at 77 K and others at 4.2 K. Numbers for spectrum b indicate the terminal levels of J for the $^5D_4 \rightarrow {}^7F_J$ transitions of Tb^{3+}. The luminescence spectra c and d were reported in ref 6.

triplet luminescence for the highly symmetrical polyoxometalates with Lindqvist or Keggin structure was extremely small due to the small disparity between excited and ground state electronic configurations, as demonstrated by $[NBu_4]_2[M_6O_{19}]$ (M = W and Mo) and $K_5[BW_{12}O_{40}]\cdot 15H_2O$.[6] Both the extremely low value of Φ_{et} $[(6 \pm 1) \times 10^{-3}]$ and the strong temperature dependence of the luminescence yield (Figure 9) for **6** are attributed to a large deactivation of the O→M lmct states with a strong temperature dependence. The condensed double Keggin structure for the $[(GeTi_3W_9O_{37})_2O_3]^{14-}$ with the approximate symmetry of D_{3h} (Figure 2b) involves the large W−O−W, Ti−O−W, and Eu−O−W bond angles of more than 150° (especially Eu−O−W bond angles of about 165°, as shown in Table 3) in the anion framework.[8,12] The strong deactivation of the O→M lmct states for the $[(GeTi_3W_9O_{37})_2O_3]^{14-}$ ligand is reflected by low values of both quantum yield and quenching temperature for the O→M lmct triplet emission of $K_9H_5[(GeTi_3W_9O_{37})_2O_3]\cdot 16H_2O$. As shown in Figure 11a, $K_9H_5[(GeTi_3W_9O_{37})_2O_3]\cdot 16H_2O$ solid exhibits a broad green emission spectrum peaking at 570 nm at low temperatures, $T < 150$ K, under 248-nm light excitation. The quantum yields of this green emisison due to the O→M lmct triplet states are extremely low, $(4.9 \pm 0.2) \times 10^{-3}$ at 4.2 K and $(1.0 \pm 0.1) \times 10^{-3}$ at 100 K. Decay time measurements of the green emission of the $K_9H_5[(GeTi_3W_9O_{37})_2O_3]\cdot 16H_2O$ solid show two-exponential decay times (due to two $^3T_{1u}$ triplet states):[6] 91 ± 6 and 140 ± 10 μs at 4.2 K and 10 ± 2 and 30 ± 4 μs at 100 K. On the other hand, the Φ_{et} value (0.19 ± 0.01) for **5** at 4.2 K is not as low as expected for the highly symmetrical $[Nb_6O_{19}]^{8-}$ ligands (Figure 2), although the strong dependence of Φ_{et} due to thermal deactivation is observed (Table 4). This is associated with two factors. One is the distortion of the $[Nb_6O_{19}]^{8-}$ ligand coordinating Eu^{3+} as a heptadentate ligand: the point symmetry of each of the three heptadentate $[Nb_6O_{19}]^{8-}$ ligands is reduced to C_{2v} from the idealized O_h symmetry.[7,20] Another is the slightly small bond angles (about 142°) of the Eu−O(μ_2)−Nb linkages compared with other polyoxometalloeuropates (Table 3).

O→M lmct Triplet Energy Transfer. One can remark that the Φ_{et} value at 77 K [$=(0.48 \pm 0.04)$] for the edge-sharing MoO_6 octahedral polyoxomolybdoeuropate **3** is small compared with the edge-sharing WO_6 octahedral polyoxotungstoeuropate **1**. This arises from the deactivation of the O→Mo lmct states in part due to the large Eu−O−Mo bond angles of about 150° for **3**.[2c,e] In addition, this may be explained by a small spin−orbit coupling of the MoO_6 octahedra, which would decrease the yield of the O→M lmct triplet states compared with the WO_6 octahedra.[6] The involvement of the O→M lmct triplet energy transfer in the polyoxometalate lattices has been investigated with three isostructural Anderson complexes $K_{5.5}H_{1.5}[SbW_6O_{24}]\cdot 6H_2O$, $Na_5[IMo_6O_{24}]\cdot 3H_2O$, and $Na_3H_6[CrMo_6O_{24}]\cdot 8H_2O$:[6] the photoexcitation of the O→M lmct bands for the former two complexes led to the broad emission due to the $^3T_{1u} \rightarrow {}^1A_{1g}$ transition originating from the O→M lmct triplet states. The green emission of $K_{5.5}H_{1.5}[SbW_6O_{24}]\cdot 6H_2O$ was intense and observed even at room temperature in contrast to $Na_5[IMo_6O_{24}]\cdot 3H_2O$, giving orange emission at low temperatures only below 100 K. Small values of the quantum yield of emission of $Na_5[IMo_6O_{24}]\cdot 3H_2O$ compared with $K_{5.5}H_{1.5}[SbW_6O_{24}]\cdot 6H_2O$ are attributed to a small spin−orbit coupling of the former with a resultant increase in the nonradiative $^1T_{1u} \rightarrow {}^1A_{1g}$ transition probability. On the other hand, $Na_3H_6[CrMo_6O_{24}]\cdot 8H_2O$, in which a central Cr^{3+} exerted several energy levels within the O→Mo lmct emission bands, did not show any O→Mo lmct triplet emission but sharp $^2T_1$, $^2E \rightarrow {}^4A_2$ lines known as R-lines from the excited Cr^{3+} with a single-exponential decay as a result of the energy transfer from the $^3T_{1u}$ O→Mo lmct states. If the singlet energy transfer of the O→Mo lmct is operative in this case, one would expect the coexistence of both O→Mo lmct triplet and Cr^{3+} luminescence, since the rate of the intersystem crossing for the $^1T_{1u} \rightarrow {}^3T_{1u}$ conversion is high enough to compete with the rate of the energy transfer to Cr^{3+}. Then, the rate of the triplet energy transfer in $Na_3H_6[CrMo_6O_{24}]\cdot 8H_2O$ was estimated to be more than 10^6 s^{-1}; otherwise the O→Mo lmct triplet emission of $Na_3H_6[CrMo_6O_{24}]\cdot$-

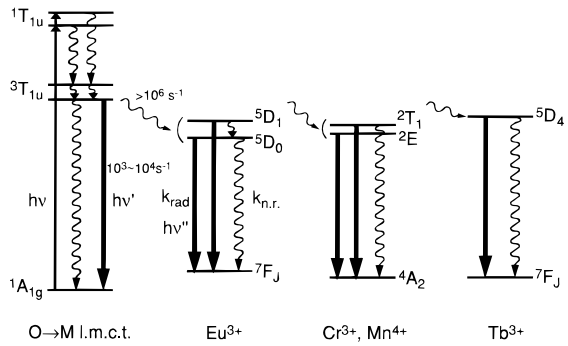

Figure 12. Summary of possible transport processes of the excitation energy of the O→M lmct in the polyoxometalate lattices. The energy levels of the O→M lmct states vary with changes in both structure and metal element of the polyoxometalates.

$8H_2O$ with the nonexponential long decays of several hundred microseconds at <100 K should be observed.[6] The same is true for the polyoxometallomanganates such as $K_6Na_2[MnW_6O_{24}]\cdot 12H_2O$, $K_6[MnMo_6O_{32}]\cdot 6H_2O$, and $Na_{12}[Mn(Nb_6O_{19})_2]\cdot 50H_2O$, where the intramolecular energy transfer from the O→M (=W, Mo, or Nb) lmct triplet states into Mn^{4+} occurs to result in only luminescence of the Mn^{4+} R-line.[21] The O→M lmct triplet states were identified for the nonmolecular oxide of transition metal ions with an empty d shell by ESR studies of the luminescent state in $K_2Cr_2O_7$, YVO_4, and $CaMoO_4$ crystals at 1.2 K.[22] Since the $^5D_0 \rightarrow {}^7F_J$ transition energy of Eu^{3+} is close to the energy of the $^2T_1$, $^2E \rightarrow {}^4A_2$ transitions of Cr^{3+} and Mn^{4+}, it is reasonable to assume the involvement of the O→M lmct triplet states in the energy transfer in the polyoxometalloeuropate lattices.

For the polyoxometalloterbates the Tb^{3+} emission under O→W lmct band excitation is much stronger than under the O→Mo lmct band excitation. This supports the energy transfer from the O→M lmct triplet states. The structures of anions for $K_3Na_4H_2[Tb(W_5O_{18})_2]\cdot 20H_2O$[13] and $[NH_4]_{12}H_2[Tb_4(H_2O)_{16}(MoO_4)(Mo_7O_{24})_4]\cdot 13H_2O$ are the same as for corresponding Eu^{3+} complexes **1** and **4**, respectively. The photoluminescence spectra of the two terbate compounds were almost the same. A typical luminescence spectrum at 77 K under O→M lmct band excitation for $[NH_4]_{12}H_2[Tb_4(H_2O)_{16}(MoO_4)(Mo_7O_{24})_4]\cdot 13H_2O$ is shown in Figure 11, where the emission spectra of the O→M lmct triplet states for $K_{5.5}H_{1.5}[SbW_6O_{24}]\cdot 6H_2O$[5] and $K_6[Mo_7O_{24}]\cdot 4H_2O$[5] at 4.2 K are added for comparison. The quantum yields of Tb^{3+} emission [$^5D_4 \rightarrow {}^7F_J$ ($J = 0-6$)] under O→M lmct band excitation (at 300 nm) were 0.38 ± 0.01 at 77 K and 9×10^{-3} at 300 K for $K_3Na_4H_2[Tb(W_5O_{18})_2]\cdot 20H_2O$[23] and 7×10^{-3} at 77 K and negligibly low at 300 K for $[NH_4]_{12}H_2[Tb_4(H_2O)_{16}(MoO_4)(Mo_7O_{24})_4]\cdot 13H_2O$. As shown in Figure 11b−d, the spectral overlap between the broad orange emission (around 700 nm) of the O→Mo lmct triplet states and the f−f absorption ($^7F_6 \rightarrow {}^5D_4$ transition at 486 nm) of Tb^{3+} is smaller than the broad green emission ($\lambda_{max} \approx 520$ nm) of the O→W lmct triplet states. This implies that the energy transfer from O→Mo lmct triplet states to Tb^{3+} in the polyoxomolybdoterbate lattices should be less efficient than in the corresponding europate lattices, which show a large spectral overlap between the O→Mo lmct triplet emission and the Eu^{3+} $^7F_0 \rightarrow {}^5D_0$ absorption (at about 580 nm). Thus, the triplet energy transfer explains why the O→W lmct band photoexcitation provides a much high yield of the Tb^{3+} emission compared with the O→Mo lmct band photoexcitation. Figure 12 shows a summary of possible transport processes of the O→M lmct excitation energy in a variety of polyoxometalate lattices.

It should be noted that the O→M lmct triplet states are reaction precursors in the electron transfer to the O→M lmct excited states from alcohols as electron donors, as established by the chemically induced dynamic electron polarization (CIDEP) technique for the photoredox reaction of $[V_4O_{12}]^{4-}$, $[Mo_7O_{24}]^{6-}$, and $[W_{10}O_{32}]^{4-}$ with alcohols in solutions.[24] In conjunction with the above results, it is deduced that the O→M lmct triplet states participate in both electron transfer and energy transfer in the polyoxometalate lattices.

Acknowledgment. We acknowledge a Grant-in-Aid for Scientific Research on Priority Areas, "New Development of Rare Earth Complexes", No. 06241104, for the Ministry of Education, Science, Sports, and Culture for support of this work.

References and Notes

(1) (a) Stillman, M. J.; Thompson, A. J. *J. Chem. Soc., Dalton Trans.* **1976**, 1138. (b) Blasse, G.; Dirksen, G. J.; Zonnevijlle, F. *J. Inorg. Nucl. Chem.* **1981**, *43*, 2847. (c) Blasse, G.; Dirksen, G. J.; Zonnevijlle, F. *Chem. Phys. Lett.* **1981**, *83*, 449. (d) Ballardini, R.; Mulazzani, Q. G.; Venturi, M.; Bolletta, F.; Balzani, V. *Inorg. Chem.* **1984**, *23*, 300. (e) Ballardini, R.; Chiorboli, E.; Balzani, V. *Inorg. Chim. Acta* **1984**, *95*, 323. (f) Darwent, J.; Flint, C. D.; O'Grady, P. J. *Chem. Phys. Lett.* **1986**, *127*, 547. (g) Sugeta, M.; Yamase, T. *Bull. Chem. Soc. Jpn.* **1993**, *66*, 444.

(2) (a) Yamase, T.; Naruke, H.; Sasaki, Y. J. *J. Chem. Soc., Dalton Trans.* **1990**, 1687. (b) Yamase, T.; Naruke, H. J. *J. Chem. Soc., Dalton Trans.* **1991**, 285. (c) Naruke, H.; Yamase, T. *J. Lumin.* **1991**, *50*, 55. (d) Yamase, T.; Naruke, H. *Coord. Chem. Rev.* **1991**, *111*, 83. (e) Yamase, T. In *Polyoxometalates: From Platonic Solids to Anti-Retroviral Activity*; Pope, M. T., Müller, A., Eds.; Kluwer Academic Publishers: Dordrecht, The Netherlands, 1994; p 337.

(3) Creaser, I.; Heckel, M. C.; Neitz, R. J.; Pope, M. T. *Inorg. Chem.* **1993**, *32*, 1573.

(4) Naruke, H.; Ozeki, T.; Yamase, T. *Acta Crystallogr.* **1991**, *C47*, 489.

(5) (a) Horrocks, W. D., Jr.; Sudnick, D. *Acc. Chem. Res.* **1981**, *14*, 384. (b) Horrocks, W. D., Jr.; Sudnick, D. *Science* **1979**, *206*, 1194.

(6) Yamase, T.; Sugeta, M. *J. Chem. Soc., Dalton Trans.* **1993**, 759.

(7) Ozeki, T.; Yamase, T.; Naruke, H.; Sasaki, Y. *Inorg. Chem.* **1994**, *33*, 409.

(8) Sugeta, M.; Yamase, T. *Acta Crystallogr. C*, in press.

(9) Peacock, R. D.; Weakley, T. J. R. *J. Chem. Soc. A* **1971**, 1836.

(10) Sjöbon, K.; Hedman, B. *Acta Chem. Scand.* **1973**, *27*, 3673.

(11) Naruke, H.; Yamase, T. *Acta Crystallogr.* **1992**, *C48*, 597.

(12) Yamase, T.; Ozeki, T.; Sakamoto, H.; Nishiya, S.; Yamamoto, A. *Bull. Chem. Soc. Jpn.* **1993**, *66*, 103.

(13) Ozeki, T.; Takahashi, M.; Yamase, T. *Acta Crystallogr.* **1992**, *C48*, 1370.

(14) Ofelt, G. S. *J. Chem. Phys.* **1963**, *38*, 2171.

(15) Blasse, G.; Grabmaier, B. C. In *Luminescent Materials*; Springer-Verlag: Berlin, Heidelberg, 1994; p 100.

(16) (a) Blasse, G. *Adv. Inorg. Chem.* **1990**, *35*, 319. (b) Van Dijk, J. M. F.; Schuurmans, H. F. H. *J. Chem. Phys.* **1983**, *78*, 5317.

(17) Blasse, G. *Prog. Solid State Chem.* **1988**, *18*, 79.

(18) (a) Blasse, G. In *Handbook on the Physics and Chemistry of Rare-Earths*; Gschneider, K. A., Jr., Eyring, L., Eds.; North-Holland: Amsterdam, 1979; p 237. (b) Verweg, J. W. M.; Dirksen, G. J.; Blasse, G. *J. Noncryst. Solids* **1988**, *107*, 49.

(19) Blasse, G. *Eur. J. Solid State Inorg. Chem.* **1991**, *t.28*, 719.

(20) Naruke, H.; Yamase, T. *Acta Crystallogr.* **1996**, *C52*, 2655.

(21) Yamase, T.; Kobayashi, T.; Kettle, S. F. A. *J. Electrochem. Soc.* **1996**, *143*, 1678.

(22) (a) Van Der Boel, W. A. J. A.; Noort, M.; Herbich, J.; Coremans, C. J. M.; Van Der Waals, J. H. *Chem. Phys. Lett.* **1984**, *103*, 245. (b) Van Der Boel, W. A. J. A.; Herbich, J.; Van Der Waals, J. H. *Chem. Phys. Lett.* **1984**, *104*, 253. (c) Barendswaads, W.; Van Der Waals, J. H. *Mol. Phys.* **1986**, *67*, 651. (d) Barendswaads, W.; Van Der Waals, J. H. *Mol. Phys.* **1986**, *59*, 337. (e) Barendswaads, W.; Van Tol, J.; Weber, R. T.; Van Der Waals, J. H. *Mol. Phys.* **1989**, *67*, 651. (f) Van Tol, J.; Van Hulst, J. A.; Van Der Waals, J. H. *Mol. Phys.* **1992**, *76*, 547. (g) Van Tol, J.; Van Der Waals, J. H. *Mol. Phys.* **1992**, *76*, 567.

(23) Ozeki, T.; Yamase, T. *J. Alloys Compd.* **1993**, *192*, 28.

(24) Yamase, T.; Ohtaka, K. *J. Chem. Soc., Dalton Trans.* **1994**, 2599.